# Supplementary Information

# E-beam-enhanced solid-state mechanical amorphization of α-quartz: Reduced deformation barrier via localized excess electrons as network modifiers

Sung-Gyu Kang[1,+], Wonseok Jeong[2,+], Jeongin Paeng[1,+], Hwangsun Kim[1], Eunsol Lee[1], Gyeong-Su Park[1], Seungwu Han[1], and Heung Nam Han[1], In-Suk Choi[1]

[1] Department of Materials Science and Engineering & Research Institute of Advanced Materials, Seoul National University, Seoul, Republic of Korea

[2] Lawrence Livermore National Laboratory, Livermore, USA

* Corresponding author: Prof. Heung Nam Han and Prof. In-Suk Choi

E-mail: hnhan@snu.ac.kr and insukchoi@snu.ac.kr

[+] These authors equally contributed to this work.

## Supplementary Figures

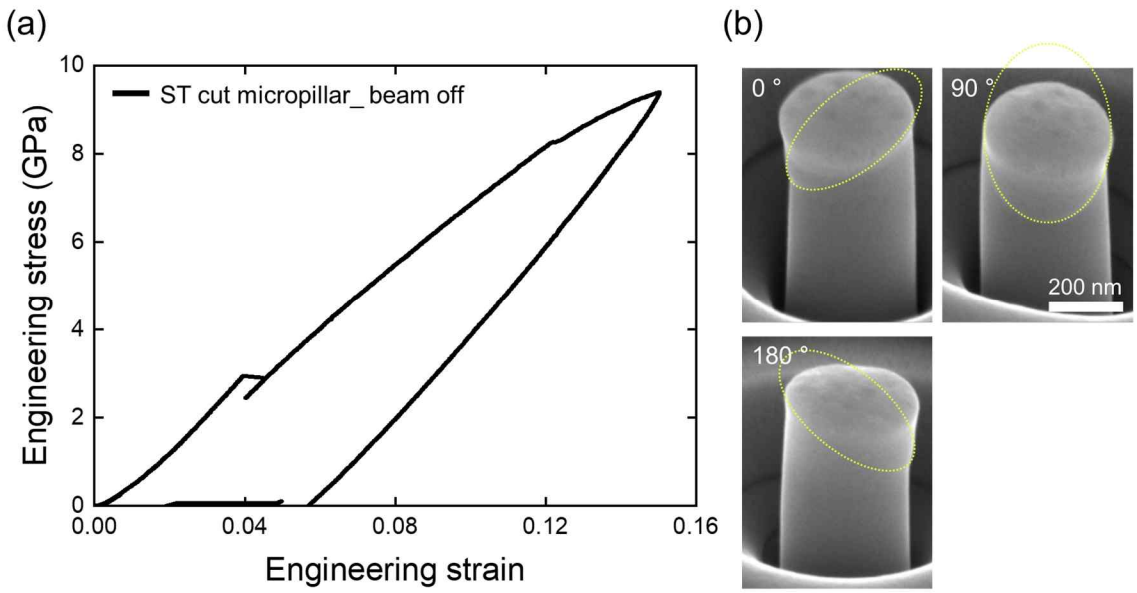


**Figure S1.** In situ SEM compression tests of ST cut α-quartz submicron pillar without e-beam. (a) Engineering stress–strain curves of pillar. (b) SEM images of compressed pillar viewed from various angles. Yellow dotted lines indicate the slip traces at the surface. We prepared a ST-cut single crystalline α-quartz substrate and fabricated pillars via FIB milling with an axial orientation of approximately $[10\bar{1}1]$. The stress-strain curve exhibits a clear pop-in event, and the compressed images reveal a surface slip trace, indicating that dislocations moved and escaped the material. By taking into account the angle between the loading direction and the axial orientation of the pillar, the basal $(0001) < \bar{1}2\bar{1}0 >$ system is estimated to be the operative slip system. Consequently, we infer that the permanent deformation of the α-quartz pillar with the axial orientation of $[0001]$ in Figure 1 does not occur via operative slip systems.

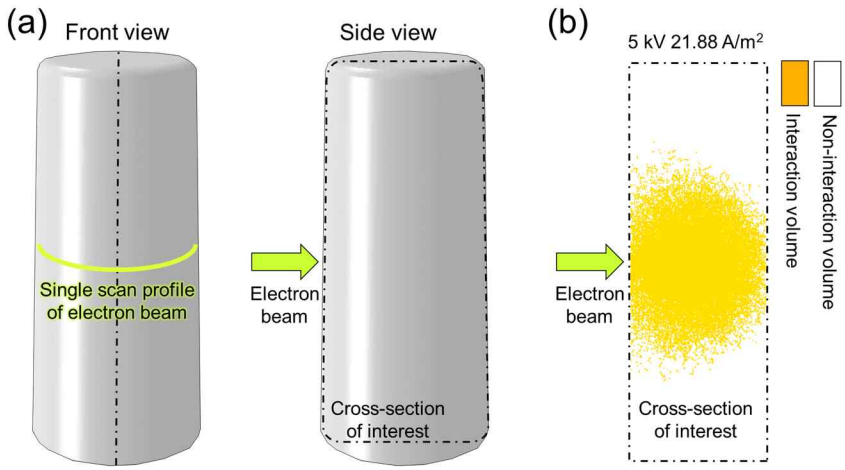


**Figure S2.** Monte Carlo simulation of electron–matter interaction in α-quartz submicron pillar.

(a) Schematic diagram of the model and cross section used for the interaction volume analysis.

(b) Interaction volume in the cross section normal to single line scan profile of the e-beam.

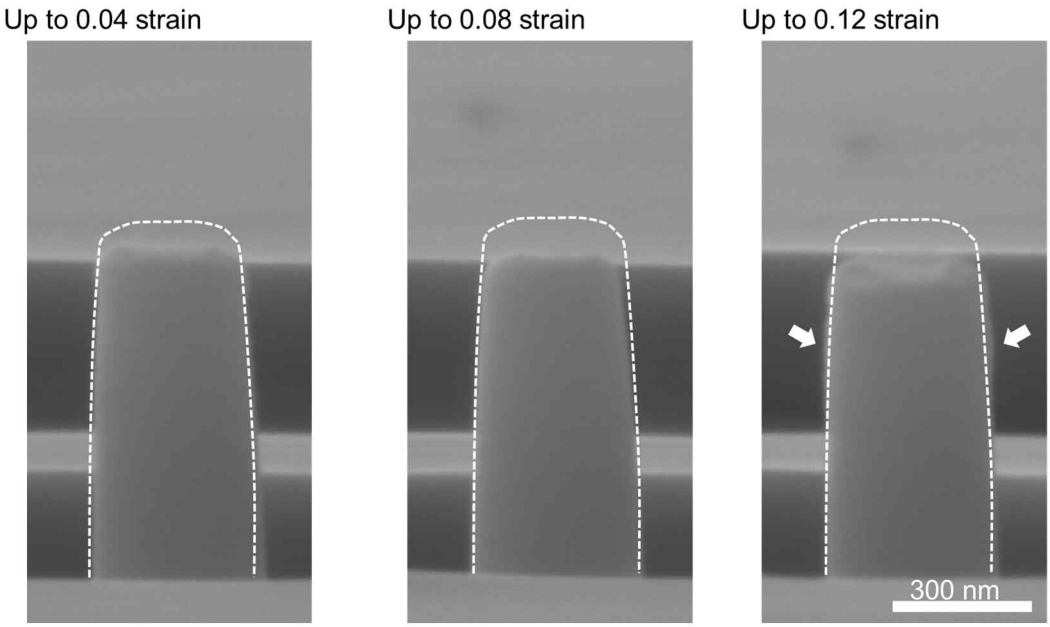


**Figure S3.** SEM images of α-quartz submicron pillars compressed to 0.04, 0.08, and 0.12 engineering strain under the irradiation of 5-kV, 21.88-A/m$^2$ electron beam. White dashed line indicates the original shape of pillar. White arrows indicate transverse deformation.

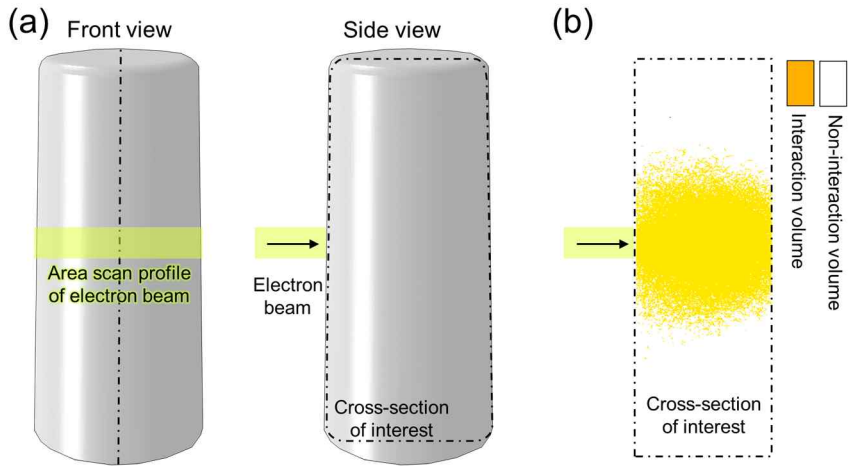


**Figure S4.** Monte Carlo simulation of electron–matter interaction in α-quartz submicron pillar with limited e-beam irradiation. (a) Schematic diagram of the model and cross section used for the interaction volume analysis. (b) Interaction volume in the cross section normal to the e-beam.

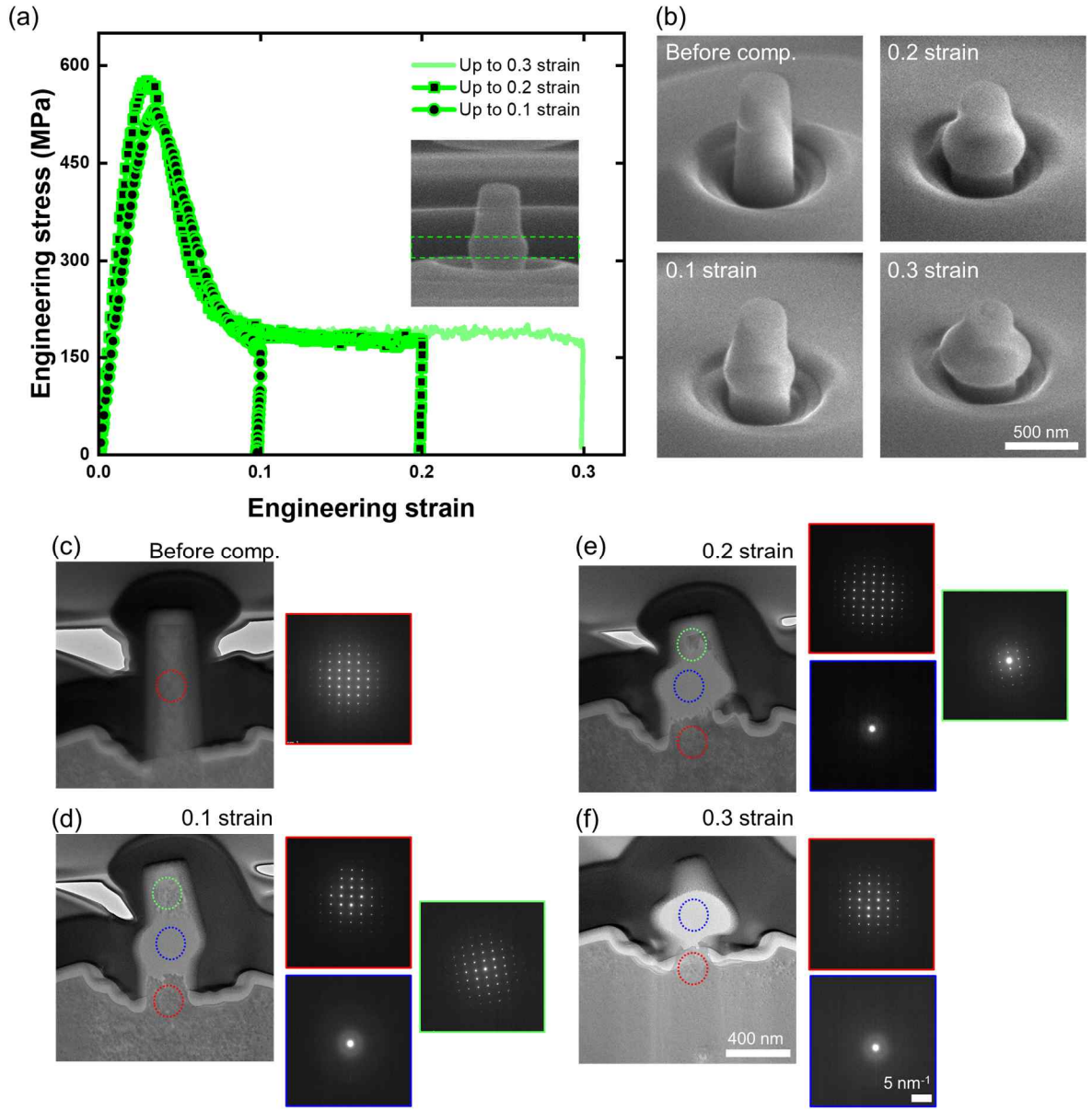


**Figure S5.** In situ SEM compression tests of α-quartz submicron pillar with and without e-beam. (a) Engineering stress–strain curves of micropillars compressed to strains of 0.1, 0.2, and 0.3. The inset image shows the e-beam irradiated area. (b) SEM images of micropillars. (c-f) Bright field images and selected area diffraction patterns of compressed α-quartz micropillar. The stress-strain curves show a similar trend to those in the original manuscript, with a maximum stress and a plateau. The SEM images in (b) indicate that the permanent deformation mainly occurred around the e-beam-irradiated area. The TEM image of the undeformed

micropillar showed negligible contrast change throughout the structure, and the diffraction pattern confirmed that the micropillar was single crystalline α-quartz. As the deformation progressed, a region with different contrast appeared inside the micropillar, and the diffraction pattern confirmed that this region corresponded to a mechanically amorphized area.

Based on the Monte Carlo simulation (Figure S4), we changed the e-beam irradiation profile so that the e-beam irradiation area and the resulting electron–matter interaction volume is confined to a specific region, without any inclination angle. The *in situ* experiments and subsequent TEM analysis confirm that the amorphized area is not the oblique shape but is almost identical to the electron–matter interaction volume in the α-quartz pillar.

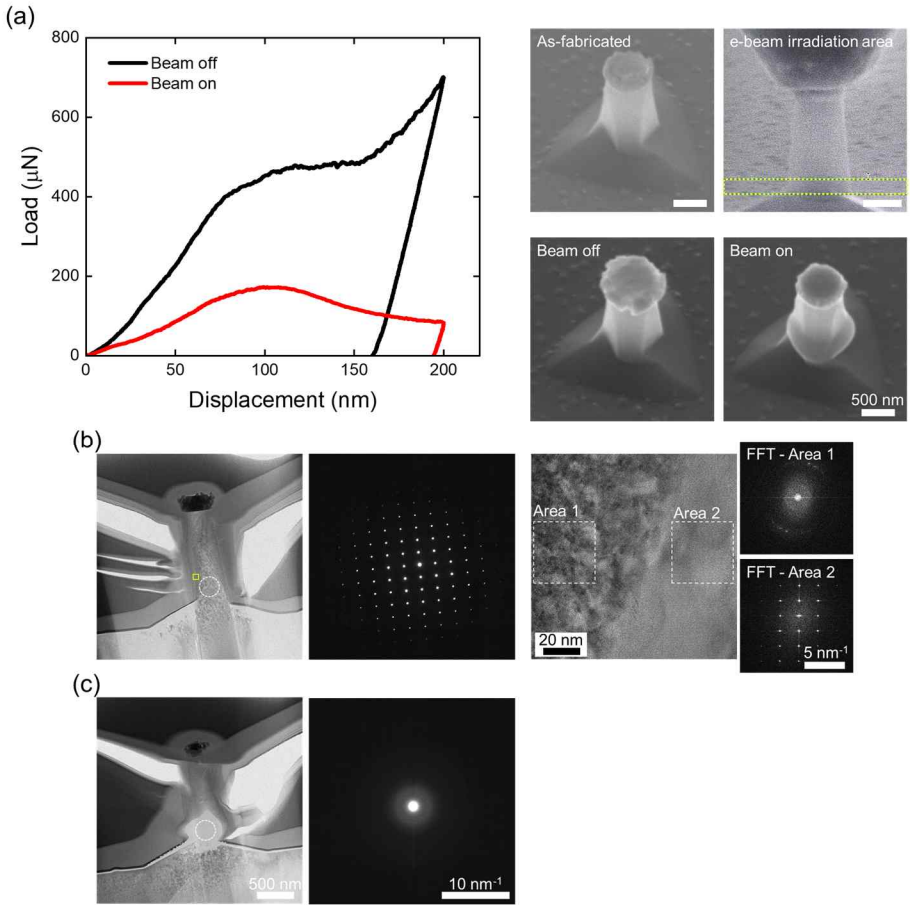


**Figure S6.** In situ SEM nanoindentation of α-quartz micropillar fabricated by wet etching process. (a) Compressive stress-strain curves with and without e-beam (10 kV, 1770 A/m$^2$) irradiation and tilted SEM images of micropillars before and after the compression. (b, c) Bright field TEM images and selected area diffraction patterns of α-quartz micropillars before and after the compression under the e-beam irradiation.

We prepared the (0001) quartz substrate and cleaned it acetone, isopropyl alcohol, and deionized water via ultrasonication. A positive photoresist TDMR-AR87 was coated on the substrate via spin coating at 4500 rpm for 60 seconds. The substrate was baked at 113℃ for 90sec on a hotplate and was developed in AZ300MIF developer for 60 seconds. To create dot-patterned metal arrays, a layer of Cr (20 nm) and Au (200 nm) was deposited by an electron beam evaporator at a rate of 1Å/s and 3Å/s rate, respectively. The resist was then removed in

acetone via ultrasonication for 30 seconds, resulting in metal arrays with dots of 0.75μm in diameter and a spacing of 50μm. The substrate was etched in a solution mixture of HF (49%): $NH_4F$ (40%) = 2: 3 at 80℃ for 260sec, then followed by rinsing with DI water. A tilted SEM image of as-fabricated micropillar in (a) shows that the pillar has metal layers on the top (20 nm of Cr and 200 nm of Au). Bright field TEM image and selective area diffraction pattern in (b) show that the α-$SiO_2$ micropillar is mostly crystalline phase. Importantly, the high resolution TEM images and corresponding Fourier transform patterns indicate the crystalline $SiO_2$ right next to the platinum layer, meaning that there is almost no amorphous layer on the surface of the pillar.

The stress-strain curves of chemically etched micropillars show analogous trend to that of FIB-milled submicron pillars, except that the micropillar compressed without the e-beam irradiation shows increased plasticity. The SEM image of the micropillar compressed without the e-beam irradiation confirms that most of the permanent deformation occurred in the metal layers on top of the micropillars. On the other hand, the SEM image of the micropillar compressed with the e-beam irradiation shows that most of the permanent deformation occurred in the e-beam irradiated area. Bright field TEM image and selected area diffraction pattern in (c) show that in the heavily deformed area the α-$SiO_2$ changed to amorphous $SiO_2$, suggesting that the mechanical amorphization occurred during the compression with the e-beam irradiation.

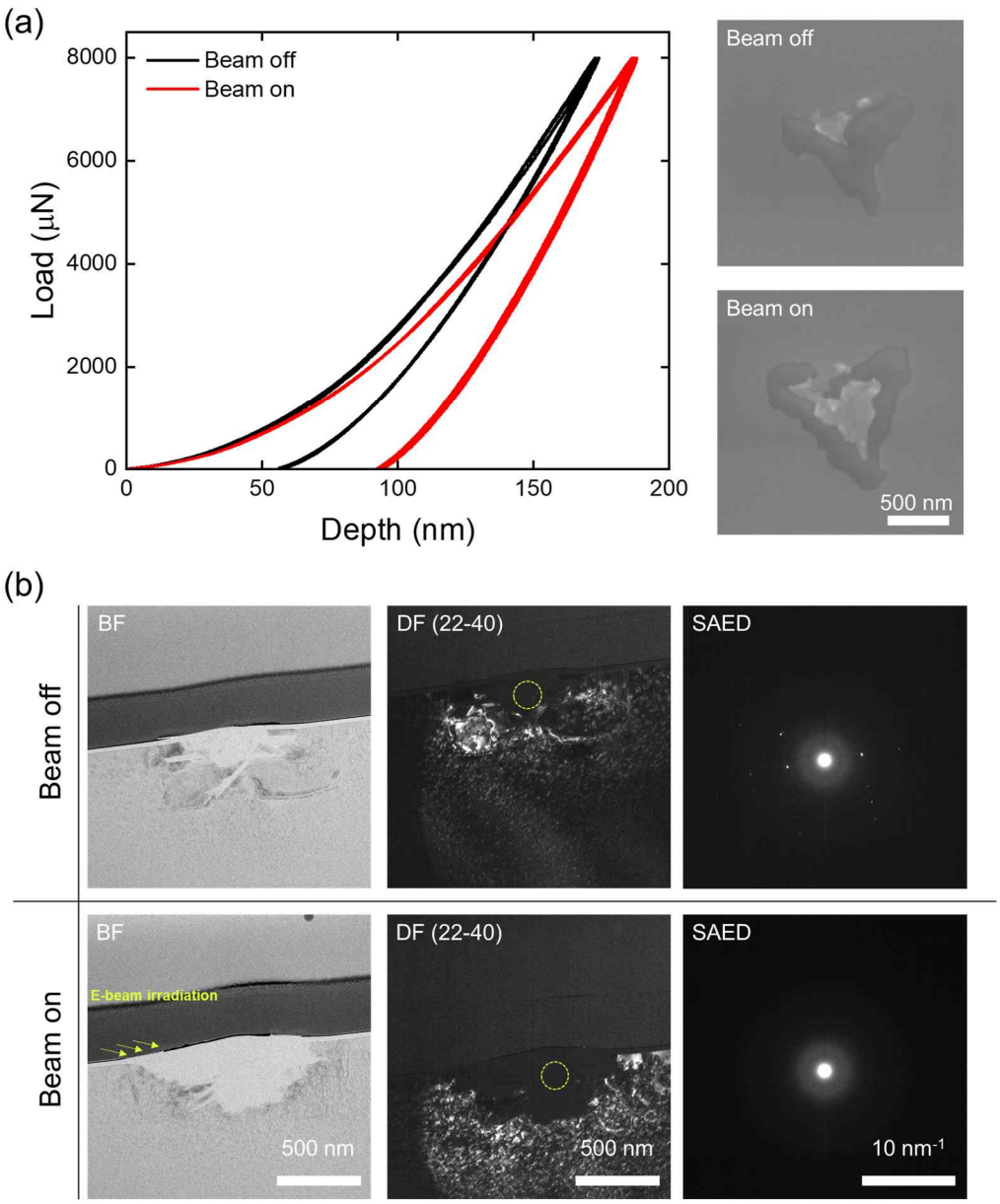


**Figure S7.** In situ SEM nanoindentation of α-quartz substrate with and without e-beam. (a) Indentation load-depth curves with SEM images of α-quartz substrates after the indentation. (b) Bright field, dark field TEM images and selected area diffraction patterns of α-quartz substrates after the indentation. We performed *in situ* SEM nanoindentation on the α-quartz (**0001**) substrate using Berkovich indenter and analyzed the cross-section of the indented area via TEM. As presented in (a), the indentation load-depth curve with e-beam irradiation (10 kV, 150 A/m$^2$)

exhibited a larger residual depth (~100 nm) compared to that without e-beam irradiation (~50 nm). The bright field (BF) and dark field (DF) TEM images of the indented area in (b) revealed that the area with different contrast is larger in the sample compressed with the e-beam irradiation than without it, and the diffraction patterns confirmed that the region with different contrast corresponds to the mechanically amorphized area.

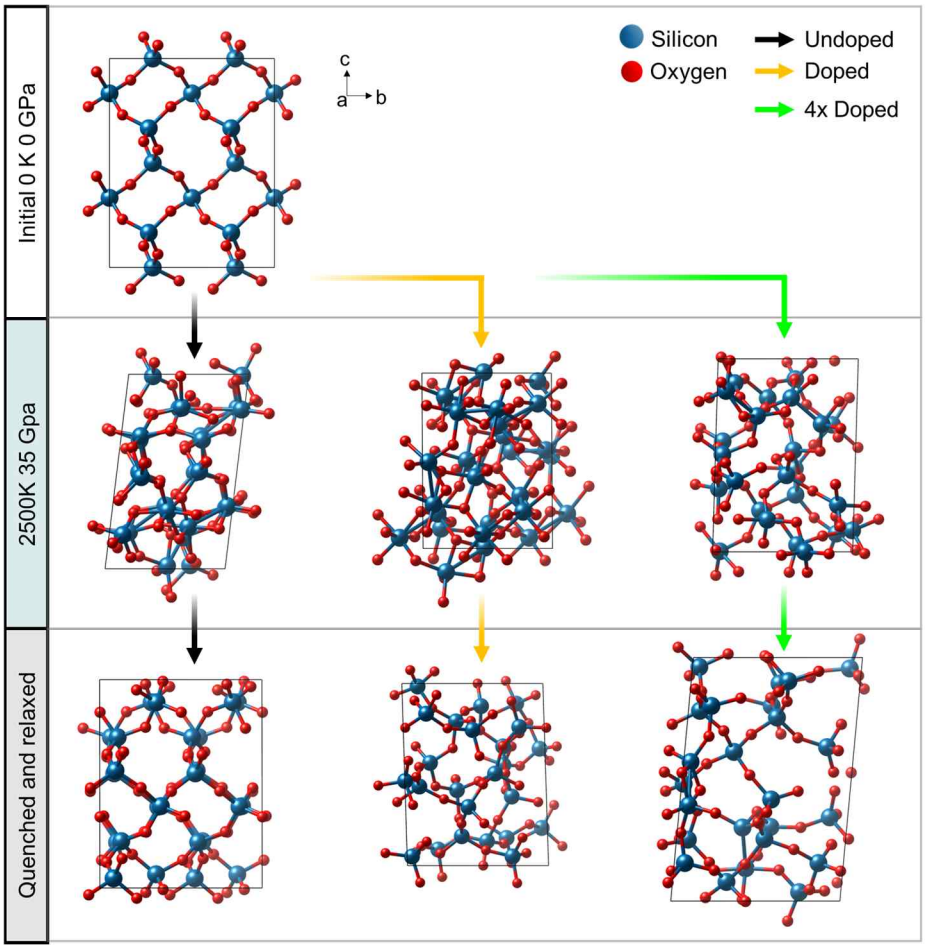


**Figure S8.** Atomic configurations of α-quartz (viewed from a axis). Blue and red circles indicate Si and O atoms, respectively.

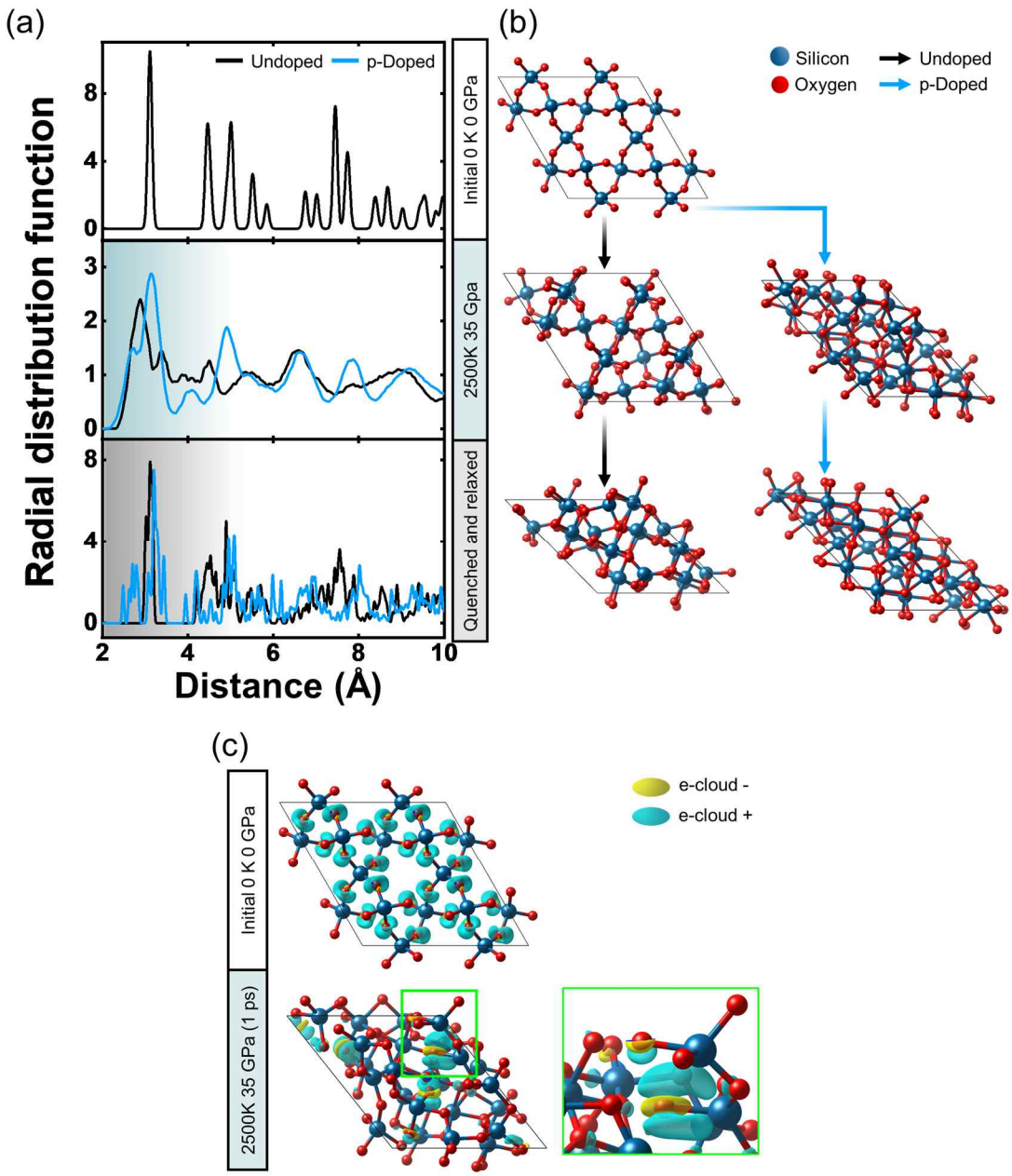


**Figure S9.** Density functional theory simulation of α-quartz under hydrostatic pressure with and without excess holes. (a) Radial distribution function (RDF) plot of an Si-Si pair in α-quartz. (b) Corresponding atomic configurations of α-quartz. (c) Atomic configurations under hydrostatic pressure with charge difference. Blue and red circles indicate Si and O atoms, respectively. Yellow and blue clouds indicate excess electrons and holes, respectively.

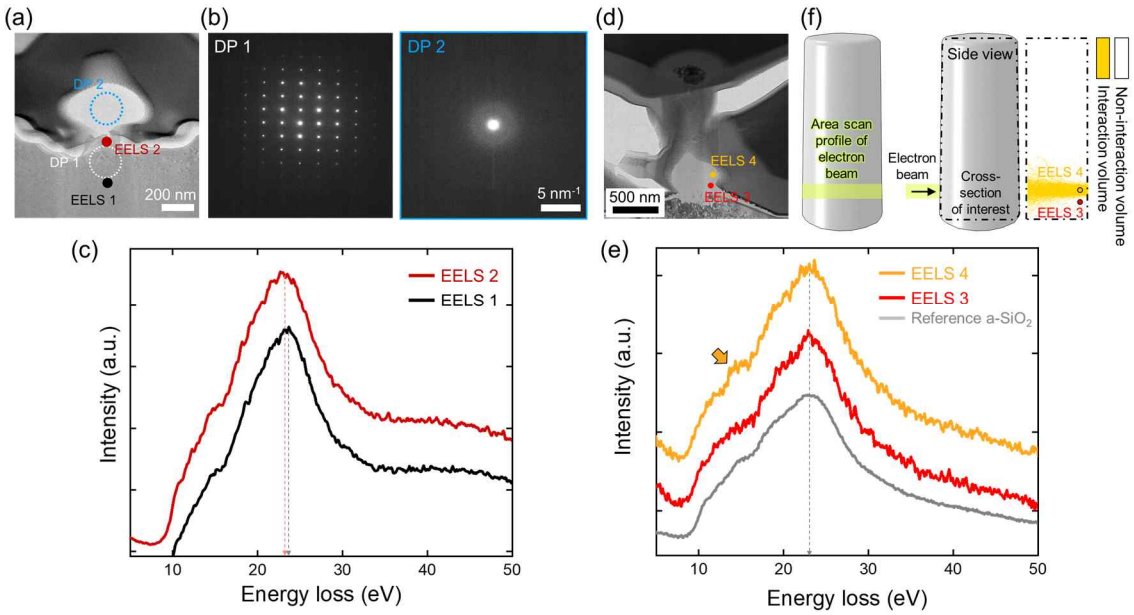


**Figure S10.** TEM analysis of α-quartz submicron pillar after the compression. (a) Bright field image of compressed α-quartz pillar (Positions of obtained diffraction pattern and EELS signals are indicated). (b) Diffraction patterns from the compressed α-quartz pillar. (c) EELS spectra obtained from the substrate and the bottom part of compressed α-quartz pillar. (d) Bright field image of compressed α-quartz pillar (Positions of obtained EELS signals are indicated). (e) EELS spectra obtained from the amorphized regions of compressed α-quartz pillar. (f) Monte Carlo simulation of electron–matter interaction in α-quartz submicron pillar.

The structural information obtained experimentally also demonstrates that the e-beam irradiation allows for a highly distorted atomic structure. We obtained STEM/EELS spectra from the mechanically amorphized pillar compressed with the e-beam irradiation. Specifically, low energy EELS spectra dominated by collective excitations was obtained at four locations: the undeformed substrate (EELS 1), the slightly deformed bottom of the pillar (EELS 2), and the heavily deformed regions of the pillar which is far (EELS 3) and near (EELS 4) from the e-beam irradiated surface. The TEM image and the corresponding diffraction patterns in (a, b)

signify that heavily deformed region is amorphous, and the bottom of the pillar maintains the crystallinity. (c) shows the low-loss EELS spectra which is dominated by bulk plasmon excitations. The dominant bulk plasmon peak of EELS 1 is centered at 23.8 eV, while the peak of EELS 2 is centered at 23.2 eV. Considering the plasmon peak of amorphous $SiO_2$ (23 eV), the slight shift of plasmon peak can be attributed to the atomic structure change towards the amorphous structure. The STEM-EELS spectra measured from the amorphized regions of the pillar, particularly far (EELS 3) and near (EELS 4) from the e-beam irradiated surface (d) are presented in (e). Distances from the irradiated surface to position EELS 3 and position EELS 4 are about 170 nm and 50 nm, respectively. The dominant bulk plasmon peaks of EELS 3 and EELS 4 are centered at ~23 eV that is the plasmon energy of amorphous $SiO_2$. On the other hand, we can observe the presence of a shoulder at ~15 eV (orange arrow) that can be related to the Si plasmon. This result strongly suggests an overall inhomogeneity in composition at the amorphized position EELS 4. The Monte Carlo simulation of electron–matter interaction volume (f) implies the number of excess charges at the EELS 4 position to be higher than at EELS 3. From the FPMD results (Figure 3(a)), we found that the newly generated Si–Si peaks appeared only in the 4×doped structure and not in the 1×doped structure, and we hypothesized that the higher the number of excess charges is, the lower the repulsion force between Si–Si or O–O atoms is. Therefore, it can be inferred that the inhomogeneity of composition in EELS 4 is caused by the new Si–Si bonds created by the presence of excess charge enabling the atomic structure distortion such as interpenetration of the $SiO_4$ tetrahedra.

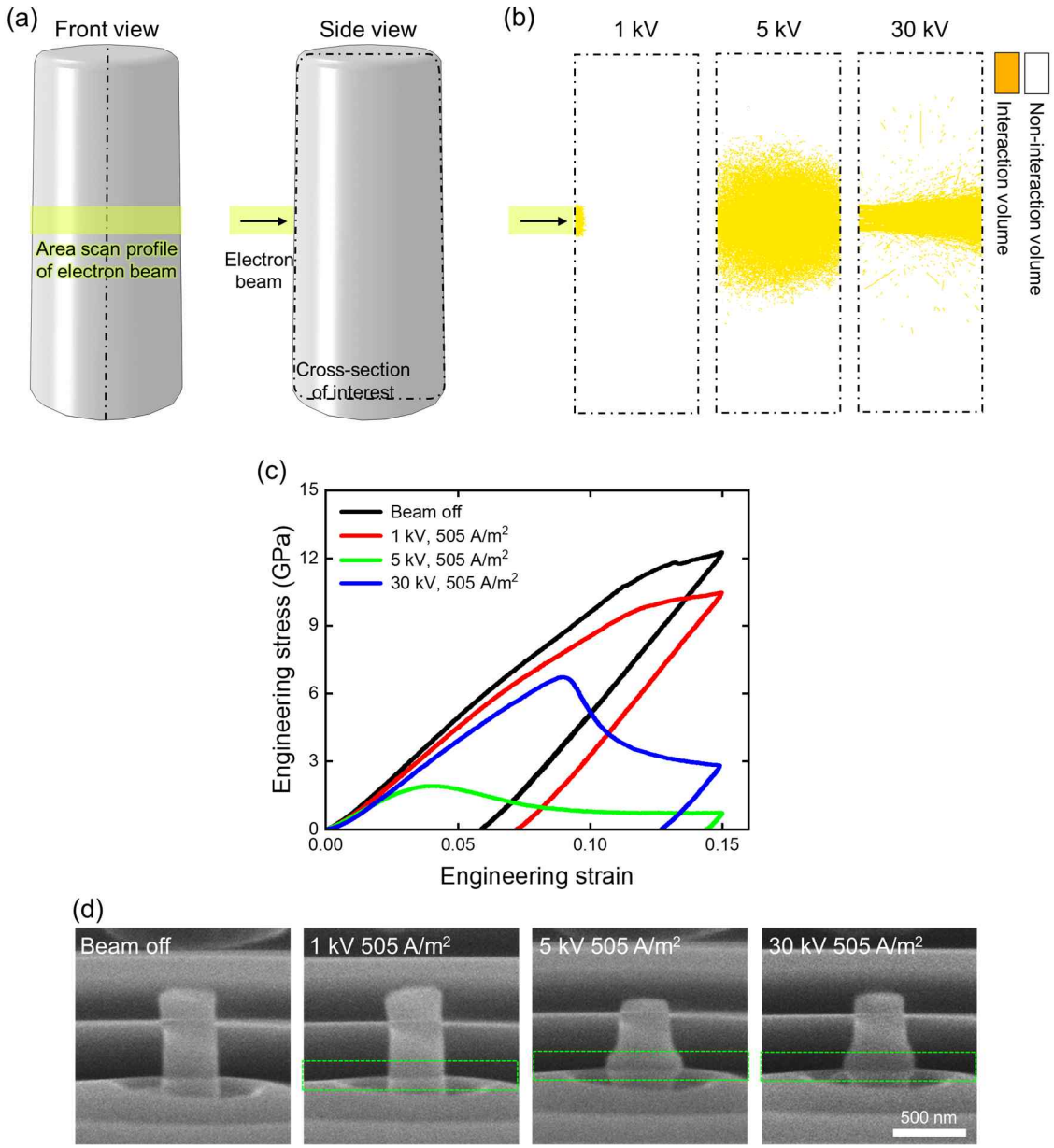


**Figure S11.** Acceleration voltage dependency of mechanical amorphization behavior of α-quartz submicron pillar. (a) Schematic diagram of the Monte Carlo simulation model and cross section used for the interaction volume analysis. (b) Interaction volume in the cross section normal to the e-beam with 1, 5, and 30 kV acceleration voltage. (c) Engineering stress–strain curves of pillars under the irradiation of e-beams with various acceleration voltages. (d) SEM images of compressed pillars. Boxes with green dashed line indicate the e-beam irradiated area.

The Monte Carlo simulation in (a, b) shows the electron–matter interaction volume was smallest for $V_A$ = 1 kV, while it was largest for $V_A$ = 5 kV due to the increasing penetration depth and the decreasing scattering angle of incident electrons with $V_A$. These simulation results suggest that α-quartz pillars may exhibit the strongest and weakest e-beam-induced deformation under $V_A$ = 5 and 1 kV, respectively. The stress-strain curve at $V_A$ = 1 kV is similar to that without e-beam irradiation, but with a slightly lower stress level. The stress-strain curves at $V_A$ = 5 and 30 kV show maximum stress and reduced plateau stress, but the stress level is much lower at $V_A$ = 5 kV. Moreover, the largest permanent deformation occurred around the e-beam irradiated region at $V_A$ = 5 and 30 kV. In contrast, only the top part of the pillars was squashed by compression under no e-beam irradiation and at $V_A$ = 1 kV, suggesting a strong electron–matter interaction volume dependency of mechanical amorphization of α-quartz under the e-beam irradiation.